Finite Elements in Analysis and Design 256 (2026) 104525

Contents lists available at ScienceDirect

Finite Elements in Analysis & Design

journal homepage: www.elsevier.com/locate/finel

An accurate coarse mesh-based analysis approach for nonlinear bending and post-buckling problems of plates and shells utilizing recurrent neural networks with Bayesian regularization back-propagation algorithm

Tan N. Nguyen [a,*], Tan Khoa Nguyen [b,c], Suppakit Eiadtrong [d,e], Nuttawit Wattanasakulpong [d,e], Mohamed-Ouejdi Belarbi [f,*], Nader M. Okasha [g], Masoomeh Mirrashid [g], Aman Garg [h,i,*]

[a] Department of Architectural Engineering, Sejong University, Seoul 05006, Republic of Korea
[b] Institute of Research and Development, Duy Tan University, 550000, Da Nang, Viet Nam
[c] Faculty of Civil Engineering, Duy Tan University, 550000, Da Nang, Viet Nam
[d] Department of Mechanical and Robotic Engineering, School of Engineering and Technology, Walailak University, Thasala, Nakhon Si Thammarat, 80160, Thailand
[e] Center of Excellence for Sustainable Disaster Management, Walailak University, Nakhon Si Thammarat, 80160, Thailand
[f] Laboratoire de Recherche en Génie Civil, LRGC, Université de Biskra, B.P. 145, R.P., 07000 Biskra, Algeria
[g] Department of Civil Engineering, College of Engineering, Abu Dhabi University, P.O. Box: 1790, Al Ain, United Arab Emirates
[h] Department of Civil Engineering and Smart Cities, Shantou University, Shantou 515063, China
[i] Department of Multidisciplinary Engineering, The NorthCap University, Gurugram, Haryana, 122017, India

ARTICLE INFO

Keywords:
Element meshes
NARX-BNNs
Nonlinear bending
Post-buckling
Plates and shells

ABSTRACT

The fineness of element meshes strongly affects the accuracy and cost of solutions in computational mechanics. In this regards, an accurate coarse mesh-based analysis approach (CMA) for nonlinear bending and post-buckling problems of plates and shells utilizing nonlinear autoregressive exogenous Bayesian neural networks (NARX-BNNs) is first proposed in this work. The CMA approach comprises two pivotal stages. Initially, a coarse mesh-based post-buckling isogeometric analysis is executed, yielding a preliminary equilibrium path quickly. The path includes a series of initial displacements and a series of initial loads. Subsequently, in the second stage, two initial series serve as the inputs for the trained networks to accurately predict displacements and loads. Finally, the resulting network outputs are a series of accurate displacements and a series of accurate loads leading to the attainment of an accurate equilibrium path. NARX-BNN is known as a recurrent neural network model utilizing Bayesian regularization back-propagation algorithm which can result in good generalization for difficult or noisy data sets. The post-buckling analyses were based on isogeometric analysis (IGA) and first-order shear deformation shell theory (FSDT) utilizing the von Karman assumption. Instabilities of shells considered in this work were snap-through, softening–hardening, and snap-back. High generalization, fast training and exactness of the proposed data-driven models were confirmed via solving five problems. The power, wide application, high exactness and effectiveness of the CMA approach for nonlinear bending and post-buckling problems of plates and shells were demonstrated. The concept of CMA approach can be applied and extended to a great number of

* Corresponding authors.
E-mail addresses: tnnguyen@sejong.ac.kr (T.N. Nguyen), mo.belarbi@univ-biskra.dz (M.-O. Belarbi), aman@stu.edu.cn, amangarg@ncuindia.edu (A. Garg).

https://doi.org/10.1016/j.finel.2026.104525
Received 24 October 2025; Received in revised form 7 January 2026; Accepted 30 January 2026
Available online 6 February 2026

problems in computational mechanics which uses element meshes in the numerical procedure to save time and labor.

1. Introduction

Structural nonlinear analysis relies on the assumption that structures behave non-linearly. Their responses are not proportional to the applied loads. *Nonlinear analysis* is more realistic, necessary and accurate than linear analysis. Hence, it is applied to many structural problems that include cracking, contact, large deformation, plasticity, instability, and other related phenomena. This paper focuses on nonlinear bending and post-buckling problems of plates and shells. As known, load–displacement equilibrium paths are often considered as the results of these problems. One of the major challenges of solving nonlinear bending and post-buckling problems using numerical methods is the requirement of a huge amount of computation and high computational cost because too many iterations in an analysis. This challenge becomes more significant in large problems with millions degrees of freedom. Another challenge of solving post-buckling problems is the divergence in several certain instances when the load–displacement curve passes the limit points. To surmount the above challenges, many nonlinear techniques have been proposed and developed to decrease iterations, computation, and to successfully pass the limit points including the Newton–Raphson and modified Newton–Raphson techniques [1,2], the modified Riks technique [3], the iterative techniques using areas [4] and optimization [5], the Koiter and accelerated Koiter techniques [6,7], the Koiter–Newton technique [8,9], a novel method using governing equations [10], a general path-following technique [11], an improved Newton technique [12], dynamic relaxation techniques [13,14], an iterative technique without predictor [15], multi-point techniques [16]. Although many nonlinear techniques have been proposed and developed, the issue of high computational cost remains and is not completely resolved. To resolve this issue, some nonlinear techniques and approaches based on artificial intelligence have been proposed to reduce the computational cost of nonlinear bending and post-buckling problems including artificial neural networks (ANNs) for nonlinear dynamic analysis [17], ANNs for improving the Newton technique [18], group method of data handling (GMDH) for adaptive path-following [19], GMDH for a novel analysis-prediction approach [20], ANNs for a fast analysis approach [21], ANNs for structures under shock-wave loads [22], ANNs for carbon nanotubes with geometric nonlinearities [23], physics-informed neural networks for nonlinear bending beam [24]. In which, there are some researches which used neural networks to predict load–displacement equilibrium paths [20,25]. The same disadvantage of these researches is we need to build up neural networks for each problem. In other words, the neural networks in these researches are not general and depending on the problem addressed. To completely resolve this issue, the CMA approach for nonlinear bending and post-buckling problems of plates and shells utilizing nonlinear auto-regressive exogenous Bayesian neural networks (NARX-BNNs) is first proposed in this paper. High generalization, fast training and exactness of the proposed data-driven models were confirmed via solving 5 problems. The power, wide application, high exactness and effectiveness of the CMA approach for nonlinear bending and post-buckling problems of plates and shells were demonstrated. NARX-BNN is known as a recurrent neural network model utilizing Bayesian regularization back-propagation algorithm which can result in good generalization for difficult, nonlinear or noisy data sets. NARX-NNs have many applications in various engineering fields such as for electricity price forecasting [26], for predicting marine engine performance parameters [27], for state of charge estimation of lithium-ion batteries [28], for groundwater level prediction [29], for enhanced metamodeling of nonlinear dynamic systems under stochastic excitations [30], for thermal dynamics identification of a pulsating heat pipe [31], and for response prediction of large buildings [32]. To the best of authors knowledge, this is the first paper which investigated NARX-BNNs for nonlinear problems in computational solid mechanics.

The outline of this research is as follows. The next section presents nonlinear bending and post-buckling analyses of isotropic shells. Section 3 shows the formulation upon FSDT and IGA for analyses of shells. A coarse mesh-based analysis approach for nonlinear bending and post-buckling problems of plates and shells is proposed in Section 4. Next, the numerical verification is presented and discussed in Section 5. Finally, this research is closed with some major conclusions.

2. Nonlinear bending and post-buckling analyses of isotropic shells

The analyses in the first stage of the CMA approach are upon isogeometric analysis and first-order shear deformation shell theory. The present formulation is re-utilized from research for post-buckling analysis of shells. Thus, a brief formulation is shown in this work, and the detailed one is available in [33]. The strain vectors of shells utilizing the FSDT and the von Karman assumption are [33]

$$\begin{aligned} \boldsymbol{\varepsilon} &= \left\{\varepsilon_{xx} \quad \varepsilon_{yy} \quad \gamma_{xy}\right\}^T = \boldsymbol{\varepsilon}_0 + z\boldsymbol{\kappa}_b \\ \boldsymbol{\gamma} &= \left\{\gamma_{xz} \quad \gamma_{yz}\right\}^T = \boldsymbol{\varepsilon}_s \end{aligned} \tag{1}$$

where

$$\begin{aligned} &\boldsymbol{\varepsilon}_0 = \boldsymbol{\varepsilon}_L + \boldsymbol{\varepsilon}_N; \quad \boldsymbol{\varepsilon}_L = \left\{ \begin{array}{c} u_{0,x} + \frac{w_0}{R} \\ v_{0,y} \\ u_{0,y} + v_{0,x} \end{array} \right\}; \quad \boldsymbol{\varepsilon}_N = \frac{1}{2} \left\{ \begin{array}{c} {w_{0,x}}^2 \\ {w_{0,y}}^2 \\ 2w_{0,xy} \end{array} \right\}; \\ &\boldsymbol{\kappa}_b = \left\{ \begin{array}{l} \beta_{x,x} \\ \beta_{y,y} \\ \beta_{x,y} + \beta_{y,x} \end{array} \right\}; \quad \boldsymbol{\varepsilon}_s = \left\{ \begin{array}{l} -\frac{u_0}{R} + w_{0,x} + \beta_x \\ w_{0,y} + \beta_y \end{array} \right\} \end{aligned} \tag{2}$$

$\boldsymbol{\varepsilon}_N$ is the nonlinear strain vector restated as

$$\boldsymbol{\varepsilon}_N=\frac{1}{2}\mathbf{A}\boldsymbol{\theta};\quad \mathbf{A}=\begin{bmatrix} w_{0,x} & 0 \\ 0 & w_{0,y} \\ w_{0,y} & w_{0,x}\end{bmatrix};\quad \boldsymbol{\theta}=\begin{Bmatrix} w_{0,x} \\ w_{0,y}\end{Bmatrix} \tag{3}$$

We assume that Ω is the initial shell configuration. The virtual work equation is as follows

$$\int_{\Omega}\hat{\boldsymbol{\sigma}}^T\delta\hat{\boldsymbol{\varepsilon}}\mathrm{d}\Omega=\int_{\Omega}\delta\bar{\mathbf{u}}^T\mathbf{f}_s\mathrm{d}\Omega \tag{4}$$

with the external load vector $\mathbf{f}_s=\{f_x \quad f_y \quad f_z\}^T$, $\bar{\mathbf{u}}^T=\{u_x \quad u_y \quad u_z\}$, $u_z=w_0$, and w_0 is the radial deflection. We assume that shells are under the radial load $f_z=\lambda f_0$. The virtual work equation is then restated as

$$\int_{\Omega}\hat{\boldsymbol{\sigma}}^T\delta\hat{\boldsymbol{\varepsilon}}\mathrm{d}\Omega=\lambda\int_{\Omega}\delta w_0 f_0\mathrm{d}\Omega \tag{5}$$

with the load factor λ and the stress resultant vector $\hat{\boldsymbol{\sigma}}$ computed as

$$\hat{\boldsymbol{\sigma}}=\left\{\boldsymbol{\sigma}_p \quad \boldsymbol{\sigma}_b \quad \boldsymbol{\sigma}_s\right\}^T \tag{6}$$

the in-plane stress vector is

$$\boldsymbol{\sigma}_p=\{N_x \quad N_y \quad N_{xy}\}^T=\{\int_{-h/2}^{h/2}(\sigma_x \quad \sigma_y \quad \tau_{xy})\mathrm{d}z\}^T \tag{7}$$

the bending stress vector and the shear stress vector respectively are

$$\boldsymbol{\sigma}_b=\{M_x \quad M_y \quad M_{xy}\}^T=\{\int_{-h/2}^{h/2}(\sigma_x \quad \sigma_y \quad \tau_{xy})z\mathrm{d}z\}^T \tag{8}$$

$$\boldsymbol{\sigma}_s=\{Q_x \quad Q_y\}^T=\{\int_{-h/2}^{h/2}(\tau_{xz} \quad \tau_{yz})\mathrm{d}z\}^T \tag{9}$$

The Hooke's law for isotropic shells is

$$\hat{\boldsymbol{\sigma}}=\hat{\boldsymbol{D}}\hat{\boldsymbol{\varepsilon}};\quad \hat{\boldsymbol{D}}=\begin{bmatrix}\mathbf{D}^p & \mathbf{0} & \mathbf{0}\\ \mathbf{0} & \mathbf{D}^b & \mathbf{0}\\ \mathbf{0} & \mathbf{0} & \mathbf{D}^s\end{bmatrix};\quad \hat{\boldsymbol{\varepsilon}}=\begin{Bmatrix}\boldsymbol{\varepsilon}_L\\ \boldsymbol{\kappa}_b\\ \boldsymbol{\varepsilon}_s\end{Bmatrix}+\begin{Bmatrix}\boldsymbol{\varepsilon}_N\\ \mathbf{0}\\ \mathbf{0}\end{Bmatrix} \tag{10}$$

with the generalized strain vector $\hat{\boldsymbol{\varepsilon}}$, the stress resultant vector $\hat{\boldsymbol{\sigma}}$ and

$$\mathbf{D}^p=\frac{Eh}{1-\upsilon^2}\bar{\mathbf{D}};\quad \mathbf{D}^b=\frac{Eh^3}{12(1-\upsilon^2)}\bar{\mathbf{D}};\quad \mathbf{D}^s=\kappa\frac{Eh}{2(1+\upsilon)}\mathbf{I} \tag{11}$$

$$\bar{\mathbf{D}}=\begin{bmatrix}1 & \upsilon & 0\\ \upsilon & 1 & 0\\ 0 & 0 & (1-\upsilon)/2\end{bmatrix};\quad \mathbf{I}=\begin{bmatrix}1 & 0\\ 0 & 1\end{bmatrix} \tag{12}$$

with the shear correction factor $\kappa=5/6$, Young's modulus E, and Poisson's ratio υ. In this work, we have proposed the CMA approach for nonlinear bending and post-buckling problems of plates and shells utilizing NARX-BNNs. The theoretical formulation is re-used from [33]. The present formulation is appropriate to doubly curved shells with two constant curvatures. For modeling shells more accurately and generally, the curvature at any point in shells must be considered in the formulations. In this regard, the Kirchhoff–Love shell model [34], the Solid-Shell model [35], or the geometrically exact shell model [36] can be referred to and adopted. In this paper, nonlinear bending and post-buckling problems of plates and shallow shells were solved. All structures could experience small or moderate rotation and large deformation; the von Karman assumption was thus used. However, in general case, the nonlinear strain–displacement relations should be fully considered to capture accurately nonlinear behaviors of structures such as moderate or large rotation, large deformation, small or large strain, and so on.

3. The formulation upon FSDT and IGA for nonlinear bending and post-buckling analyses of isotropic shells

The current formulation for isotropic shells is identical with the formulation for FG-CNTRC shells in [33] except a minor difference in computing the matrices for isotropic material in Eqs. (10)–(12). The system of linear incremental equations at the m^{th} load increment and the i^{th} iteration is as

$$\mathbf{K}_T(\mathbf{q}_m)\Delta^i\mathbf{q}_m={}^i\mathbf{F}_{\mathrm{ext},m}-{}^i\mathbf{F}_{\mathrm{int},m} \tag{13}$$

with the tangent stiffness matrix

$$\begin{aligned}\mathbf{K}_T=&\int_{\Omega}\left[\begin{Bmatrix}\mathbf{B}_A^L\\ \mathbf{B}_A^b\\ \mathbf{B}_A^s\end{Bmatrix}+\begin{Bmatrix}\mathbf{B}_A^N\\ \mathbf{0}\\ \mathbf{0}\end{Bmatrix}\right]^T\begin{bmatrix}\mathbf{D}^p & \mathbf{0} & \mathbf{0}\\ \mathbf{0} & \mathbf{D}^b & \mathbf{0}\\ \mathbf{0} & \mathbf{0} & \mathbf{D}^s\end{bmatrix}\left[\begin{Bmatrix}\mathbf{B}_A^L\\ \mathbf{B}_A^b\\ \mathbf{B}_A^s\end{Bmatrix}+\begin{Bmatrix}\mathbf{B}_A^N\\ \mathbf{0}\\ \mathbf{0}\end{Bmatrix}\right]\mathrm{d}\Omega+\\ &+\int_{\Omega}\left(\mathbf{B}_A^g\right)^T\begin{bmatrix}N_x & N_{xy}\\ N_{xy} & N_y\end{bmatrix}\mathbf{B}_A^g\mathrm{d}\Omega\end{aligned} \tag{14}$$

and the external load vector

$$ {}^{i}\mathbf{F}_{\text{ext},m} = ({}^{i}\lambda_m + \Delta^{i}\lambda_m)\int_{\Omega} f_0 \left\{ \begin{matrix} 0 & 0 & N_A & 0 & 0 \end{matrix} \right\}^T \mathrm{d}\Omega = ({}^{i}\lambda_m + \Delta^{i}\lambda_m)\mathbf{F}_0 \tag{15} $$

with the referenced load vector $\mathbf{F}_0$ and the non-uniform rational B-spline basic function (NURBS) N_A. The internal force vector is as [33]

$$ {}^{i}\mathbf{F}_{\text{int},m} = {}^{i}\mathbf{K}_m {}^{i}\mathbf{q}_m \tag{16} $$

with

$$ {}^{i}\mathbf{K}_m = \int_{\Omega} \left[\left\{ \begin{matrix} \mathbf{B}_A^L \\ \mathbf{B}_A^b \\ \mathbf{B}_A^s \end{matrix} \right\} + \left\{ \begin{matrix} \mathbf{B}_A^N \\ \mathbf{0} \\ \mathbf{0} \end{matrix} \right\} \right]^T \left[\begin{matrix} \mathbf{D}^p & \mathbf{0} & \mathbf{0} \\ \mathbf{0} & \mathbf{D}^b & \mathbf{0} \\ \mathbf{0} & \mathbf{0} & \mathbf{D}^s \end{matrix} \right] \left[\left\{ \begin{matrix} \mathbf{B}_A^L \\ \mathbf{B}_A^b \\ \mathbf{B}_A^s \end{matrix} \right\} + 0.5 \left\{ \begin{matrix} \mathbf{B}_A^N \\ \mathbf{0} \\ \mathbf{0} \end{matrix} \right\} \right] \mathrm{d}\Omega \tag{17} $$

The modified Riks technique [3] is chosen to solve the nonlinear equations. Therefore, an iterative procedure continues until the following convergence criterion is met as

$$ e = \frac{\left\| {}^{i}\lambda_m \mathbf{F}_0 - {}^{i}\mathbf{F}_{\text{int},m} \right\|}{\left\| ({}^{i}\lambda_m + \Delta^{i}\lambda_m)\mathbf{F}_0 \right\|} < 10^{-6} \tag{18} $$

The incremental solutions can be obtained from Eq. (13). Then, the displacement vector $\mathbf{q}$ and the load factor λ of each iteration are updated as [3]

$$ \begin{aligned} {}^{i+1}\lambda_m &= {}^{i}\lambda_m + \Delta^{i}\lambda_m \\ {}^{i+1}\mathbf{q}_m &= {}^{i}\mathbf{q}_m + \Delta^{i}\mathbf{q}_m \\ \Delta^{i}\mathbf{q}_m &= \Delta^{i}\mathbf{q}_{R,m} + \Delta^{i}\lambda_m \mathbf{q}_{F,m} \end{aligned} \tag{19} $$

where the displacement vector resulting from the reference load $\mathbf{q}_{F,m}$ and the displacement vector resulting from the residual load $\Delta^{i}\mathbf{q}_{R,m}$ computed as

$$ \begin{aligned} \Delta^{i}\mathbf{q}_{R,m} &= [\mathbf{K}_T(\mathbf{q}_m)]^{-1}({}^{i}\lambda_m\mathbf{F}_0 - {}^{i}\mathbf{F}_{\text{int},m}) \\ \mathbf{q}_{F,m} &= [\mathbf{K}_T(\mathbf{q}_m)]^{-1}\mathbf{F}_0 \end{aligned} \tag{20} $$

4. Coarse mesh-based analysis approach for nonlinear bending and post-buckling problems of plates and shells utilizing NARX-BNNs

4.1. Nonlinear auto-regressive exogenous Bayesian neural networks (NARX-BNNs)

A NARX-BNN is known as a recurrent neural network model coupled with a Bayesian regularization back-propagation algorithm. A NARX-BNN can be conceptually presented by the following equation [32]:

$$ y(t) = f\,[y(t-1), \dots, y(t-d), u(t-1), \dots, u(t-d)] + e(t) \tag{21} $$

where $y(t)$ is the model output while $y(t-1), \dots, y(t-d), u(t-1), \dots, u(t-d)$ are the model inputs. $e(t)$ is the noise term. d is number of delays or the maximum lag for the input and output. It is seen that the model needs d past values of both y and u to predict $y(t)$ at the current time. Fig. 1 shows a typical NARX-BNN model. The model includes 3 layers: input-, hidden-, and output-layers. The hidden layer contains neurons used to map the nonlinear relationship between the input data and the output data. The output of the hidden layer $y_p(t)$ and the model output $y(t)$ are computed as follows [32]:

$$ \begin{aligned} y_p(t) &= f\left(\sum_{i=1}^{K} I_{Wi} u_i + \sum_{j=1}^{K} I_{Wo} y_j + b_1 \right) \\ y(t) &= \sum_{i=1}^{K} O_{Wi} f_i + b_2 \end{aligned} \tag{22} $$

where b_1 and b_2 are the bias terms. K is the number of neurons on the hidden layer. I_{Wi} is the connection weights for u and I_{Wo} is the connection weights for y. O_{Wi} is the weights of the links connecting the output node to the nodes on hidden layer. For convenience, the weight vector $\mathbf{w} = [I_{Wi} \ \ I_{Wo} \ \ O_{Wi}]$ contains all the weights utilized in the network. f is the activation function. The activation function TANSIG is for the hidden layer while the PURELIN is for the output layer. These two functions are expressed as [37]

$$ \begin{aligned} f &= tansig\,(x) = \tfrac{2}{1+e^{-2x}} - 1 \\ f &= purelin\,(x) = x \end{aligned} \tag{23} $$

The feed-forward back-propagation (BPP) algorithm is utilized to train networks. Upon this algorithm, weights and biases of neurons can be modified numerous times to reduce the difference between the actual and desired outputs of the network. The goal

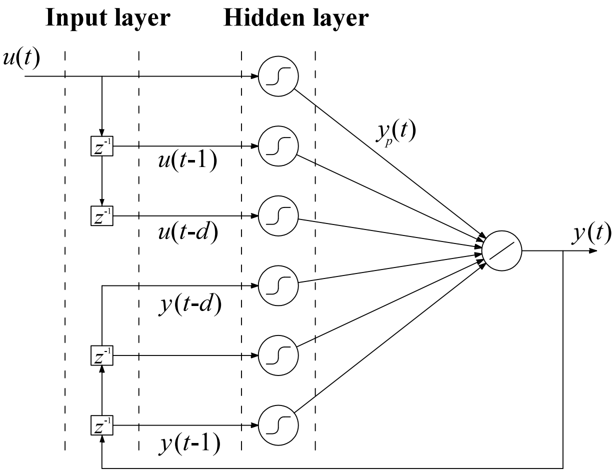

Fig. 1. A typical NARX-BNN model.

of training process is to optimize the network performance in predictions or to minimize the network's error. A stopping criterion upon the mean square error (MSE) can be utilized to evaluate the network performance. The MSE is computed as follows [37]

$$MSE = \frac{1}{N}\sum_{i=1}^{N}\left(e_i\right)^2 = \frac{1}{N}\sum_{i=1}^{N}\left(t_i - y_i\right)^2 \tag{24}$$

N is known as the total number of samples. t_i represents the target while y_i is the network's output for the ith sample. Some optimization techniques can be utilized to speed up the convergence of BPP algorithm such as the Levenberg–Marquardt technique, the scaled conjugate gradient technique, and the Bayesian regularization technique [37–39]. The Bayesian regularization technique is used in this work because of its advantages. It can lead to good generalizations for noisy, nonlinear, and difficult data sets.

4.2. Bayesian regularization back-propagation algorithm

The objective function of a network utilizing Bayesian regularization is expressed as [32,40]

$$F = \beta E_D + \alpha E_W \tag{25}$$

where the sum of squared errors E_D, the sum of squared weights E_W, and the parameters of objective function α and β. In this method, the network weights are random variables. Hence, the density function for weights is computed as follows [40]

$$P(\mathbf{w}|D,\alpha,\beta,M) = \frac{P(D|\mathbf{w},\beta,M)P(\mathbf{w}|\alpha,M)}{P(D|\alpha,\beta,M)} \tag{26}$$

where the vector of weights $\mathbf{w}$, the current model M, the data set D, the prior density $P(\mathbf{w}|\alpha,M)$, and the likelihood function $P(D|\mathbf{w},\beta,M)$. The normalization factor $P(D|\alpha,\beta,M)$ can guarantee that the total probability is one. Assume that the noises in training data and in the prior distribution are Gaussian, the probability densities can be expressed as follows [40]

$$\begin{aligned} P(D|\mathbf{w},\beta,M) &= \tfrac{1}{Z_D(\beta)}\exp(-\beta E_D) \\ P(\mathbf{w}|\alpha,M) &= \tfrac{1}{Z_W(\alpha)}\exp(-\alpha E_W) \end{aligned} \tag{27}$$

with $Z_D(\beta) = (\pi/\beta)^{N/2}$ and $Z_W(\alpha) = (\pi/\alpha)^{N/2}$. Substitute Eq. (27) to Eq. (26), one obtains [40]

$$P(\mathbf{w}|D,\alpha,\beta,M) = \frac{1}{Z_F(\alpha,\beta)}\exp(-F(\mathbf{w})) \tag{28}$$

in Bayesian regularization, the optimal weights can be found when the objective function F is minimized. Bayes' rule is now applied to optimize the parameters α and β as follows [40]

$$P(\alpha,\beta|D,M) = \frac{P(D|\alpha,\beta,M)P(\alpha,\beta|M)}{P(D|M)} \tag{29}$$

the likelihood function $P(D|\alpha,\beta,M)$ is a normalization factor in Eq. (26). This factor is determined from Eq. (26) as [32,40]

$$P(D|\alpha,\beta,M) = \frac{P(D|\mathbf{w},\beta,M)P(\mathbf{w}|\alpha,M)}{P(\mathbf{w}|D,\alpha,\beta,M)} \tag{30}$$

notably, all the probabilities have the Gaussian form. Hence, Eq. (30) is re-written as [32,40]

$$P(D|\alpha,\beta,M) = \frac{Z_F(\alpha,\beta)}{Z_D(\beta)Z_W(\alpha)} \tag{31}$$

$Z_F(\alpha, \beta)$ is determined via a Taylor series expansion as [32,40]

$$Z_F \approx (2\pi)^{N/2}(\det((\mathbf{H})^{-1}))^{1/2}\exp(-F(\mathbf{w})) \tag{32}$$

$\mathbf{H} = \beta\nabla^2 E_D + \alpha\nabla^2 E_W$ is known as Hessian matrix. Substitute this result to Eq. (31), we obtain the optimal values for α and β as [32,40]

$$\alpha = \frac{\gamma}{2E_W(\mathbf{w})} \quad \text{and} \quad \beta = \frac{N-\gamma}{2E_D(\mathbf{w})} \tag{33}$$

with the effective number of parameters $\gamma = N - 2\alpha\mathrm{tr}(\mathbf{H})^{-1}$ and the total number of parameters N. Optimization of the parameters α and β is conducted as follows [40]:

- **(0)** Initialize α, β, and the weights w.
- **(1)** Find the minimum value of the objective function F upon the Levenberg–Marquardt algorithm.
- **(2)** Determine $\gamma = N - 2\alpha\mathrm{tr}(\mathbf{H})^{-1}$, the Hessian matrix can be determined via the Gauss–Newton approximation [40]: $\mathbf{H} = \nabla^2 F(\mathbf{w}) \approx 2\beta\mathbf{J}^T\mathbf{J} + 2\alpha\mathbf{I}_N$.
- **(3)** Determine the new values of α and β via Eq. (33).
- **(4)** Steps 1 to 3 are iterated until the convergence is achieved.

The weight can be updated after each iteration of the Levenberg–Marquardt algorithm in **Step 1** as [40]:

$$w_{i+1} = w_i - (\mathbf{J}_i^T\mathbf{J}_i + \mu_i\mathbf{I})^{-1}\mathbf{J}_i^T e_i \tag{34}$$

with the unit matrix $\mathbf{I}$, the error factor e, and the learning parameter μ. The learning parameter μ equals 0.005. This value is widely used in the Bayesian regularization back-propagation algorithm. The decrease and increase factors for μ respectively are 0.1 and 10. The maximum value for μ is 1e10.

4.3. Coarse mesh-based analysis approach for nonlinear bending and post-buckling problems

4.3.1. Concept of the coarse mesh-based analysis approach

The coarse mesh-based analysis approach (CMA) contains two key stages. *In the first stage*, a coarse mesh-based post-buckling isogeometric analysis is performed. As a result, an initial equilibrium path is quickly obtained but incorrect. The path includes a series of initial displacements and a series of initial loads. *In the second stage*, two above series are considered as the inputs of two NARX-BNNs which are the trained networks for predictions of displacements and loads. The next sections show how the data is generated and the networks are trained. The obtained outputs are a series of accurate displacements and a series of accurate loads. An accurate equilibrium path is hence obtained via these two accurate series. The flow chart and description of the CMA are respectively shown in Figs. 2 and 3 for its details and illustration. As seen in Fig. 3 the initial equilibrium path, which is incorrect, becomes the accurate one upon the NARX-BNNs. The current networks utilize 1 hidden layer and a small number of neurons. Thus, time for training and applying a network is very low, about 5 s which can be neglected in computing the efficiency of the approach. Thus, the cost of the present approach is almost that in the first stage using a coarse mesh-based analysis. As known, a coarse mesh-based analysis is very fast compared to a fine mesh-based one. Therefore, the proposed approach can dramatically save the computational cost compared to conventional ones. Notably, the initial equilibrium path in Figs. 2 and 3 is the coarse-mesh equilibrium path. Series of initial displacements and series of initial loads refer to the coarse-mesh equilibrium path, not initially physical conditions.

4.3.2. Data generation and data structure

The cubic NURBS elements were utilized in this work. The coarse mesh was chosen as 6x6 elements while the fine mesh was 14x14 elements. Number of Gauss points for each element was 4x4. Fig. 4 shows 15 isotropic panels under central point load for data generation. Boundary conditions were imposed in mathematical models as follows. The clamped boundary was $u_0 = v_0 = w_0 = \beta_x = \beta_y = 0$ and the hinged boundary was $u_0 = v_0 = w_0 = \beta_y = 0$, at $x = 0, \alpha R$. Boundaries 1, 2 and 3 were respectively defined as hinged-free-hinged-free, fully clamped, and clamped-free–hinged-free. Nonlinear bending and post-buckling analyses of 15 panels were performed for data generation. The length and the radius of all the panels in this section respectively were as: $L = B = 508$ mm and $R = 2540$ mm (Geometry 1). Notably, the thickness h varied for 15 different panels as seen in Fig. 4. Young's modulus and Poisson's ratio of all the panels in this section respectively were as $E = 3.103$ kN/mm^2 and $\nu = 0.3$ (Material 1). Fig. 5 shows the data generation and data structure. There were 15 analyses of 15 panels using coarse mesh and 15 analyses of 15 panels using fine mesh. As the results of the coarse mesh-based analyses, 15 series of central deflections and 15 series of loads were achieved. Then, we assembled 15 series of central deflections to obtain 1 unified series of central deflections such as *series1 series2 series3*... *series15*. Also, we obtained 1 unified series of loads from 15 individual series of loads by assembling. Similarly for the fine mesh-based analyses, we also obtained 1 unified series of central deflections and 1 unified series of loads. Finally, the networks for deflection and for load were trained as follows. The unified series of central deflections from the coarse mesh-based analyses was considered as the input for training the network for deflection while that from the fine mesh-based analyses was the target. Similarly, the unified series of loads from the coarse mesh-based analyses was considered as the input for training the network for load while that from the fine mesh-based analyses was the target. The next section presents the necessary information of NARX-BNNs and their training and application performances.

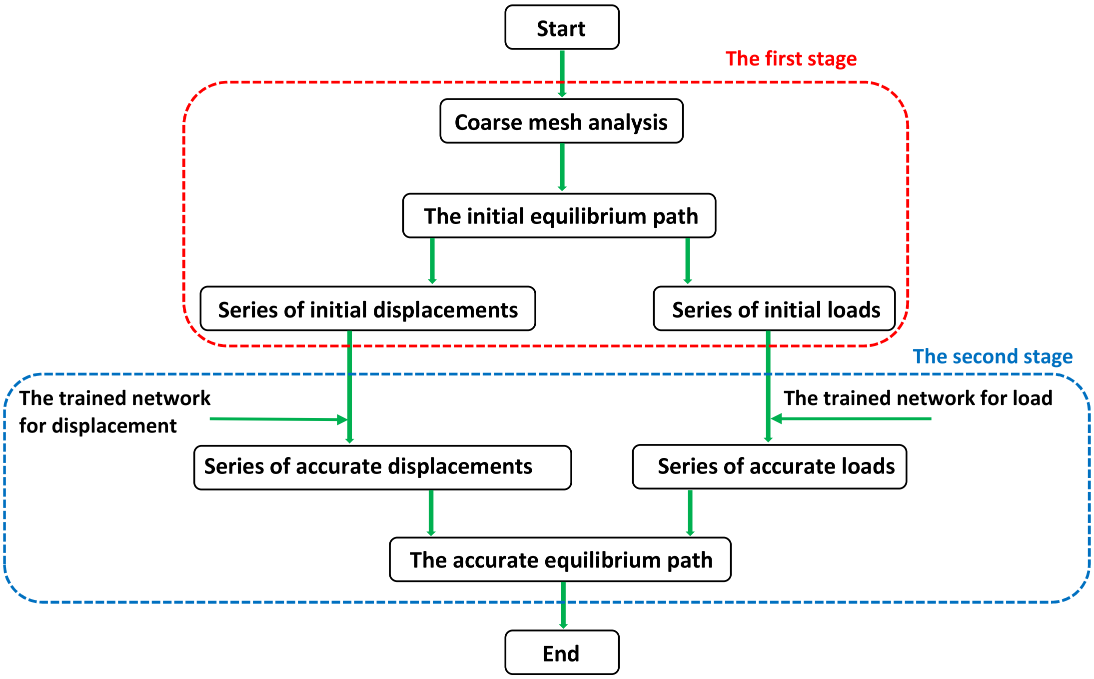

Fig. 2. Flow chart of the CMA.

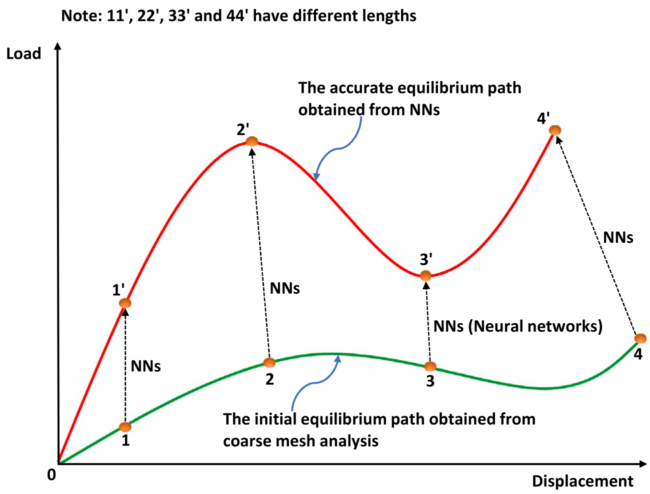

Fig. 3. Description of the CMA.

4.3.3. Training and application performances of NARX-BNNs

The network's parameters were utilized in this research as follows. The networks contained 2 layers, that were the hidden layer and the output layer. The hidden one had 10 neurons while the output one had 1 neuron. Number of delays d was fixed at 2 for all the networks. NARX-BNNs utilized the Bayesian regularization (B-R) in their training processes. The B-R had a validation mechanism integrated within it. It did not require a validation set to assess the models. Thus, the data set was only partitioned into two subsets: the testing set (15%) and the training set (85%). All the NARX-BNNs were trained and applied employing the neural network fitting application integrated in MATLAB R2021a. All the coarse and fine mesh analyses and all the training and prediction phases in this paper were performed on a CPU with the processor 13th Gen Intel(R) Core (TM) i7-13700 (2.10 GHz) and RAM 16.0 GB to compute times. Fig. 6 shows the training performances of the displacement network and the load network. The best training performances of the displacement network and the load network were respectively reached at epochs 724 and 1000 where their training processes could be stopped. Figs. 7 and 8 show the regressions of the displacement network and the load network, respectively. The regressions and the regression coefficients (R) were calculated for the training set, the testing set, and

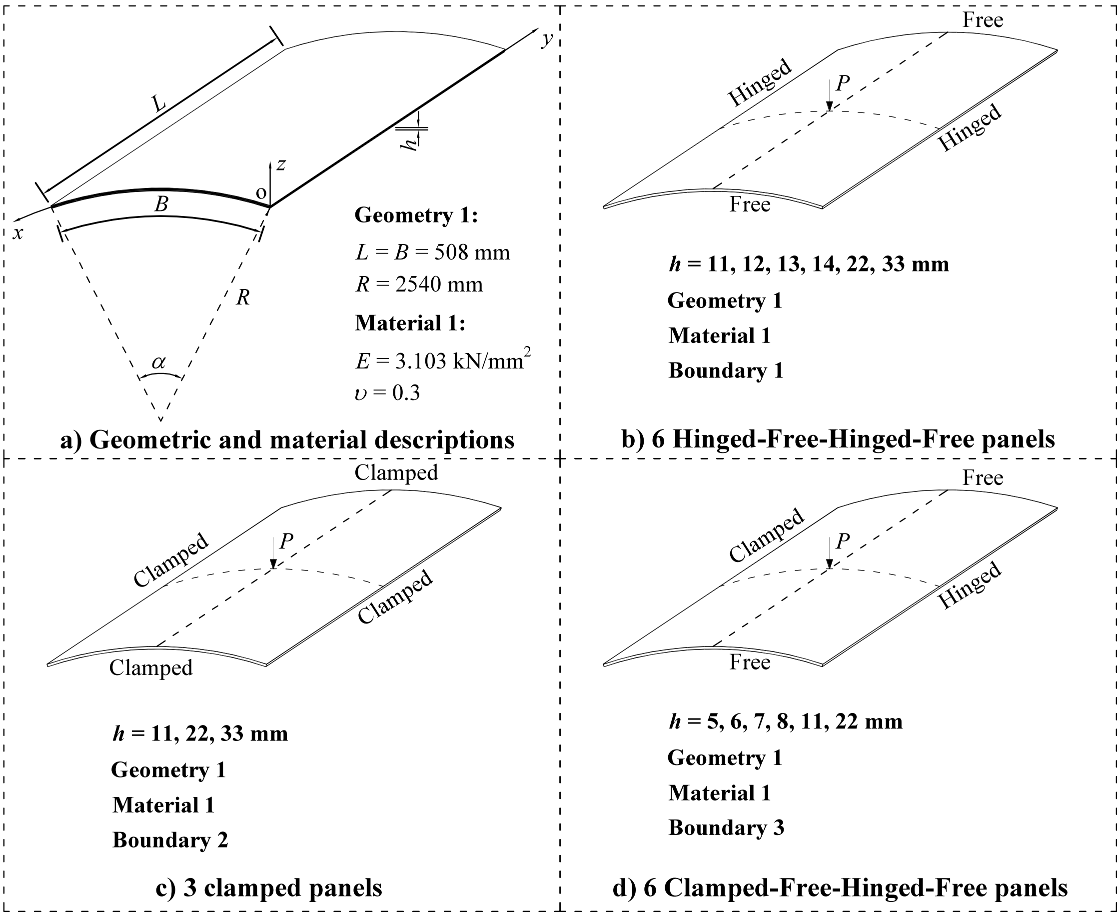

Fig. 4. 15 panels under central point load for data generation.

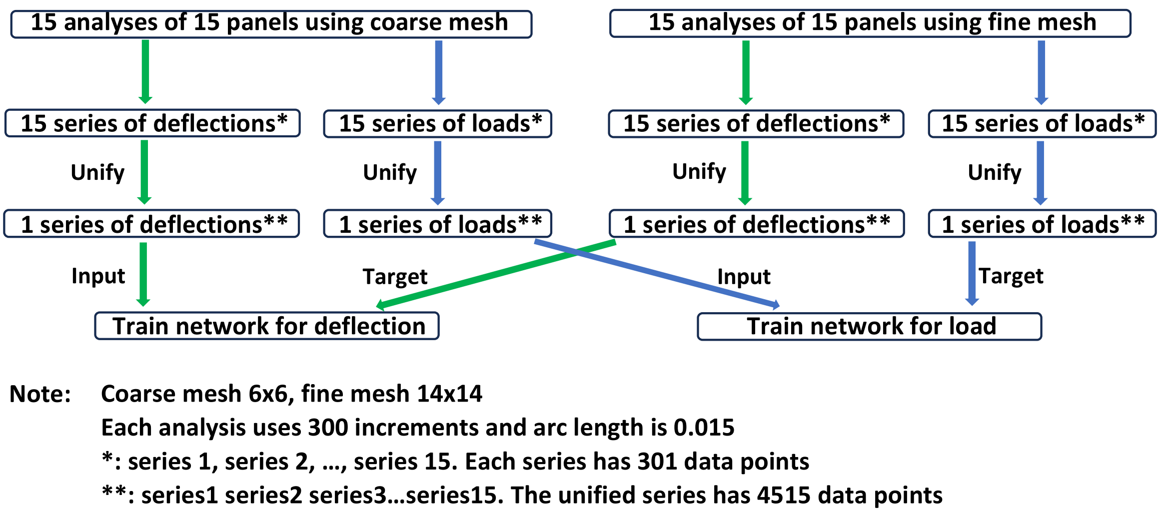

Fig. 5. Data generation and data structure.

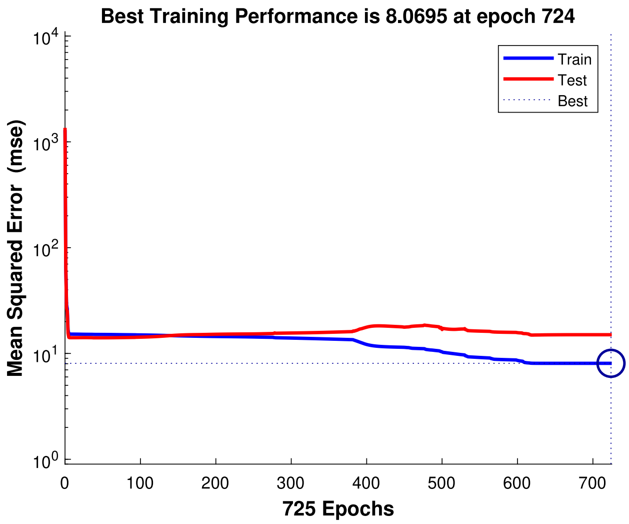

(a) The displacement network

(b) The load network

Fig. 6. Training performances of NARX-BNNs.

all data set. In addition, the fitting lines and the diagonal lines of the squares (the dashed lines) were drawn for these three data sets. As seen, all the regression coefficients were nearly equal to 1. In addition, for each data set in Figs. 7 and 8, the fitting line and the diagonal line were very close or identical. That means the outputs and the targets (or the actual values) fit very well. It can be concluded that the displacement network and the load network were well trained and produced good predictions. Notably, most of the outputs and the targets fit very well as seen in Figs. 7 and 8. That means the outputs and the corresponding targets are very close or identical. Thus, most of the points lie on the diagonal line. However, there are still some out-of-diagonal-line points. For these points, the outputs are quite different from the corresponding targets. This is a frequent problem of networks, especially when they are trained by difficult, nonlinear, or noisy data sets. The trained networks were utilized to quickly predict nonlinear bending and post-buckling behaviors of structures in the next section.

5. Numerical verification

The exactness and effectiveness of the CMA approach were demonstrated in this section. The CMA was applied to various types of structures, loading, boundaries, materials, and physical phenomenons. Five problems described in Fig. 9 were solved. In three first problems (Problems 1, 2, and 3), the geometry, loading, boundaries, and material were the same with that in the training data. The only difference was in these three problems we used the thicknesses ($h = 12.7, 25.4, 6.35$ mm) different from that in the training

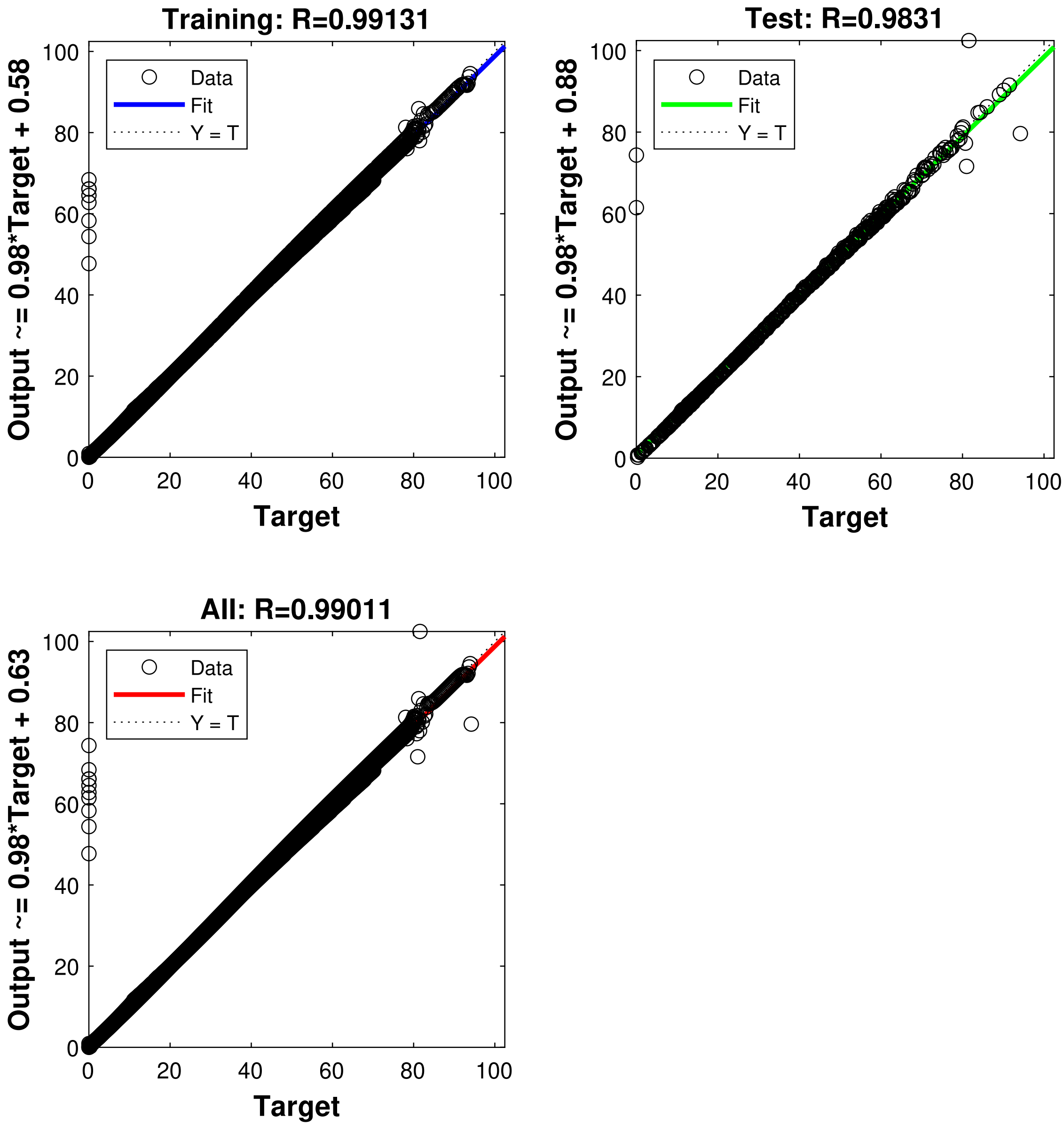

Fig. 7. Regression of the displacement network.

data. In two last problems (Problems 4 and 5), types of structures, the geometries, loading, boundaries, materials were different from that in the training data. High generalization, accuracy, effectiveness, and automation of the trained networks were confirmed via solving the above problems. The below isogeometric analysis (IGA) results were obtained by using the fine mesh 14x14 and the same formulation with that used in the first stage of the CMA approach.

5.1. The CMA approach for post-buckling problems of panels under radial point load

Problems 1, 2, and 3 described in Fig. 9 were solved in this section. As mentioned earlier in these three problems, the geometry, loading, boundaries, and material were the same with that in the training data. The only difference was in these three problems we used the thicknesses ($h = 12.7, 25.4, 6.35$ mm) different from that in the training data.

In the first problem, a hinged–hinged panel under central point load was considered. Geometry 1, material 1, and boundary 1 were the same with that in the training data. However, the thickness was $h = 12.7$ mm different from that in the training data. Fig. 10 shows the response of panel utilizing IGA with various meshes. It is seen that the results from coarse mesh (6x6) and fine mesh (14x14) are completely different. The result from fine mesh agrees well with the reference solutions using finite element method

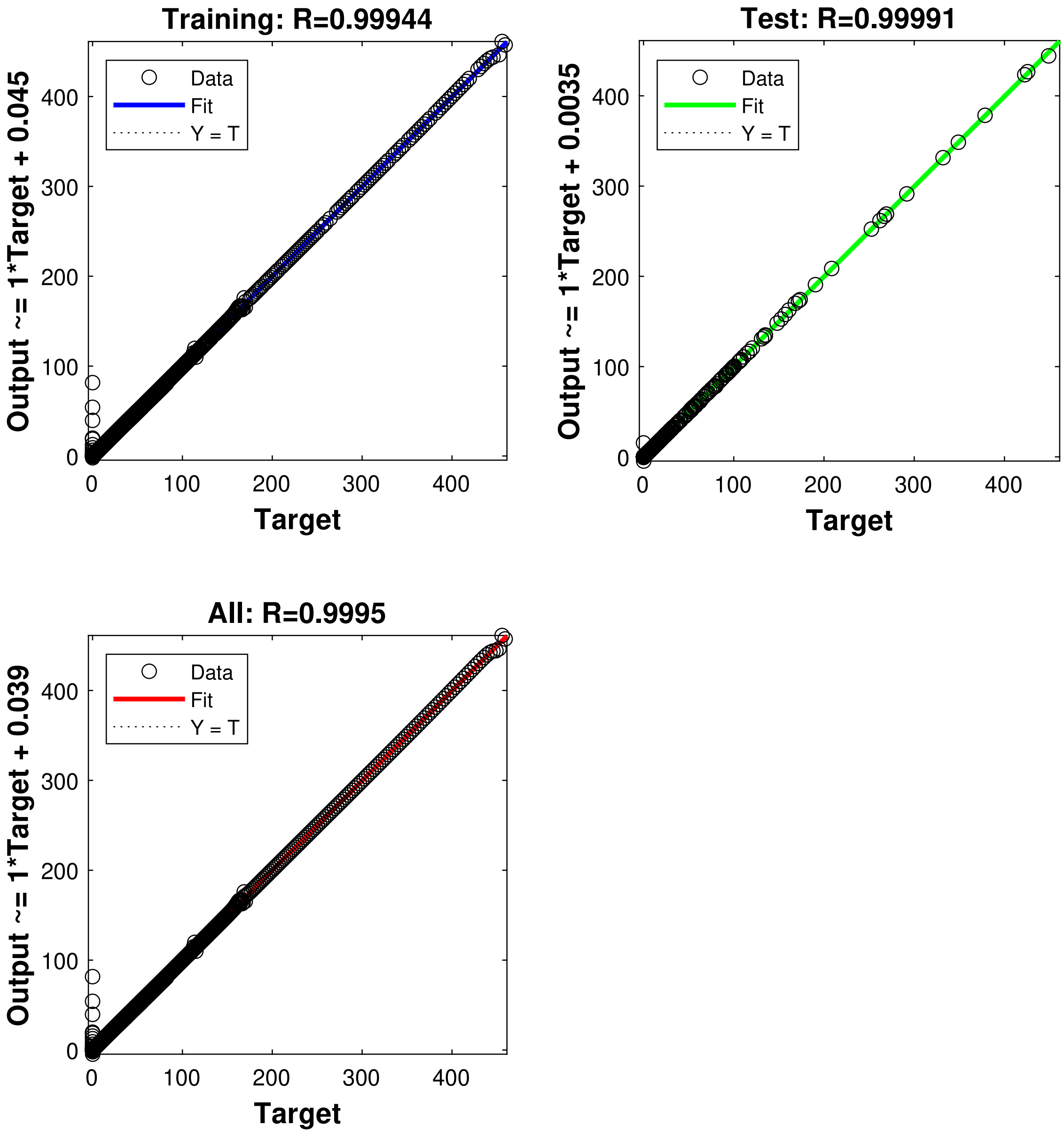

Fig. 8. Regression of the load network.

such as Crisfield [3] and Sabir [41]. High accuracy of the present formulation and solution was confirmed. The result from coarse mesh included a series of initial displacements and a series of initial loads. These two series were considered as the inputs of the trained networks for predictions of displacements and loads. The obtained outputs were a series of accurate displacements and a series of accurate loads. An accurate equilibrium path was hence obtained via these two accurate series. Fig. 11 shows the CMA solution using coarse mesh (6x6) and the IGA one using fine mesh (14x14). A good agreement was found. The current networks only utilized 1 hidden layer and 10 neurons on it. Thus, time for training and applying a network was very low. As a result, the cost of the present approach was almost that in the first stage using a coarse mesh-based analysis. Specifically, the computational cost for the CMA solution included the cost for coarse mesh (6x6) analysis with 157 load increments was 171 s, the cost for data loading for prediction was 7 s, and the cost for prediction was 1 s. In total, the computational cost for the CMA solution was 179 s while the computational cost for the IGA solution using fine mesh (14x14) and the same number of load increments was 1549 s. Clearly, the proposed approach saved 88.4% computational cost compared to the conventional one. The exactness and effectiveness of the CMA approach for post-buckling analysis of shells having the snap-through instability were demonstrated. The first problem was also solved by using an effective and efficient approach, which combined the discrete-strain gap (DSG) method and the patch-wise reduced integration in order to alleviate membrane-locking effects in quadratic NURBS-based isogeometric Kirchhoff–Love shell

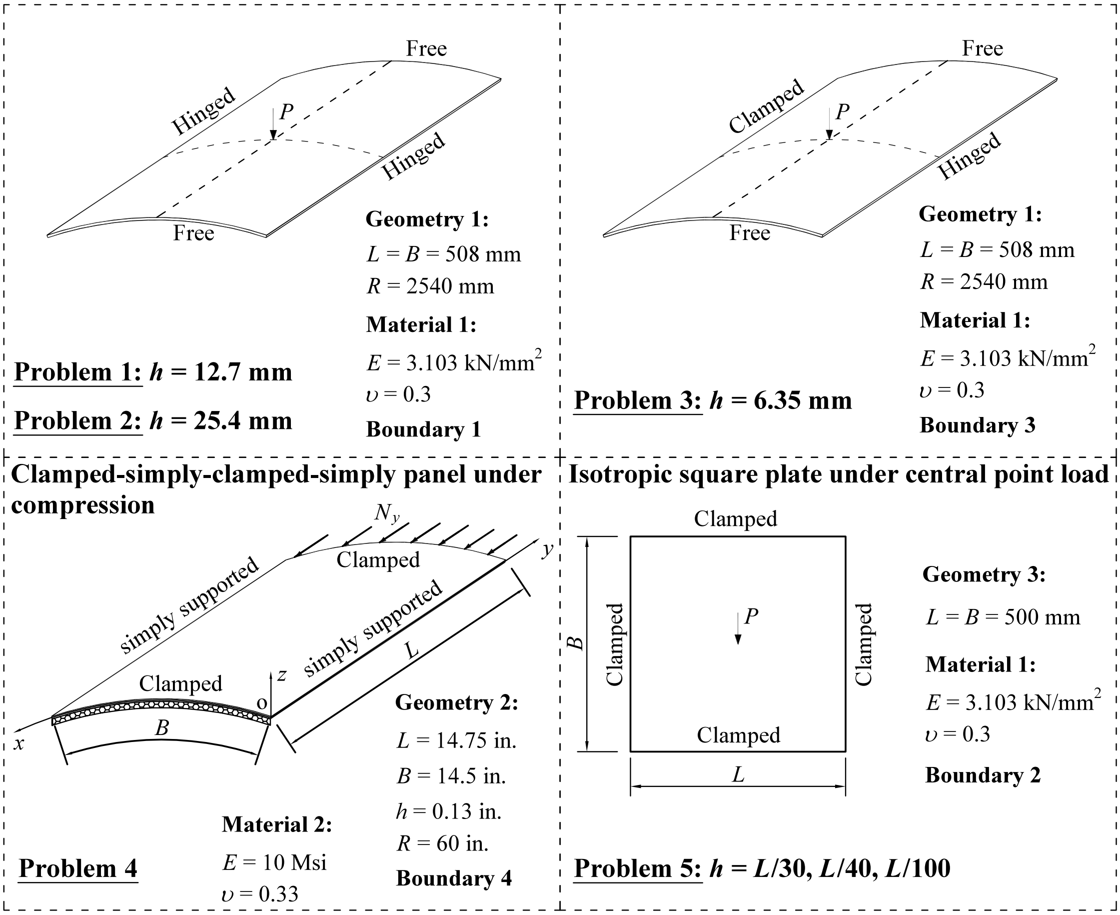

Fig. 9. Problems for verification of the CMA.

elements [42]. The approach can effectively alleviate or eliminate the membrane locking and significantly reduce computational costs through the efficient numerical integration. As a result, the approach can solve the first problem by using a very coarse mesh 5x5 elements. Next, effect of the network's structure on the CMA solution is presented in Fig. 12. The CMA solution utilizing 5 neurons was incorrect compared to the IGA one. As seen, the more number of neurons on the hidden layer, the better solution. Hence, it is recommended to employ the CMA with at least 10 neurons on the hidden layer to obtain accurate solutions. Besides, it was found that the splitting ratio just slightly affected the CMA solution. This can be explained as follows. The CMA in this paper utilized the big data (4515 data points), so the data amount was always enough for training networks with three considered splitting ratios in Fig. 12. Effect of the delay number on the CMA solution is presented in Fig. 13 in the comparison to the IGA solution. The more number of delays, the more exact solution but the higher time consuming. As seen, the CMA solution was not completely correct when delay was equal to 1. This was clearly seen when the deflection was around 20 mm. Hence, it is recommended to employ the CMA with the number of delays d is at least equal to 2 to obtain accurate solutions. Next, we investigated the CMA approach for post-buckling analysis of shells having the softening–hardening instability by solving the second problem. The description of the second problem was the same with that of the first problem except the thickness $h = 25.4$ mm. Fig. 14 shows the present solution in the comparisons with that using IGA and Sabir using FEM [41]. All the solutions matched well. In the third problem, a clamped–hinged panel under central point load was considered. The panel's thickness was $h = 6.35$ mm different from that in the training data. Fig. 15 shows the CMA and IGA solutions. Both solutions agreed well and the snap-back instability was successfully detected upon the CMA approach. It is concluded that the high exactness and effectiveness of the CMA approach for post-buckling analysis of shells having snap-through, softening–hardening, and snap-back instabilities were demonstrated.

5.2. The CMA approach for post-buckling problems of panels under axial compression

In this section, a simply supported–clamped–simply supported–clamped (CCSS-Boundary 4) panel under axial compression was considered. The problem's description is shown in Fig. 9. Notably, the material, geometry, boundary, and loading of this problem were completely different from that in the training data. Boundary conditions were imposed in mathematical models as follows.

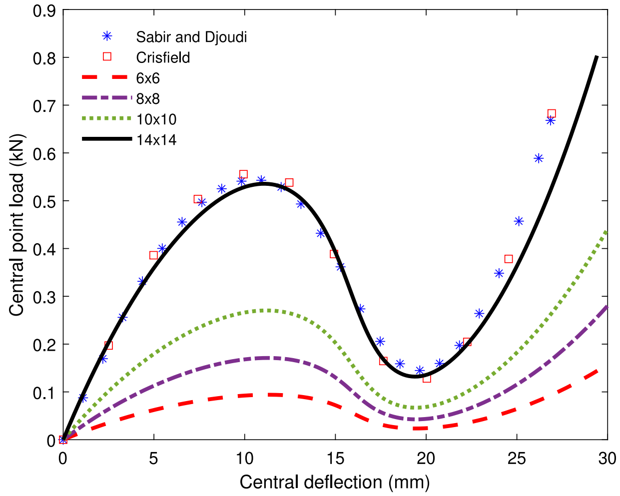

Fig. 10. Analysis of a hinged–hinged panel under central point load utilizing IGA and various meshes, $h = 12.7$ mm.

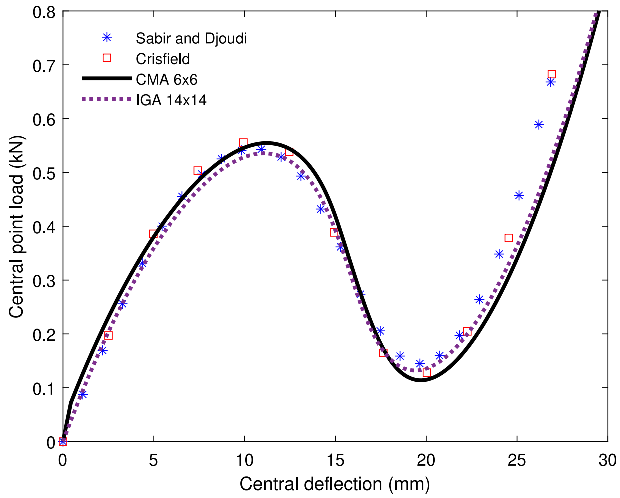

Fig. 11. Analysis of a hinged–hinged panel under central point load, $h = 12.7$ mm.

The simply supported boundary (S) was $w_0 = \beta_y = 0$ at $x = 0, \alpha R$. The clamped boundary was defined before. Fig. 16 shows the CMA and IGA solutions in the comparison with that utilizing the mesh-free kp-Ritz method (MKR) [43]. These solutions matched well.

5.3. The CMA approach for nonlinear bending problems of plates

In the last problem, a clamped isotropic square plate under central point load was considered. The problem's description is shown in Fig. 9. Notably, the training data was only generated upon the shell structures and not upon the plate ones. As known, behaviors of curved shells and flat plates are completely different. Figs. 17, 18, and 19 show the CMA and IGA solutions with various thickness ratios. Both solutions agreed very well for all cases. From the results of two last problems (Problems 4 and 5), some conclusions can be drawn as follows. High generalization and exactness of the trained networks were confirmed. Again, the exactness, effectiveness, power, and automation of the CMA approach for nonlinear bending and post-buckling problems were demonstrated.

6. Conclusions

An accurate coarse mesh-based analysis approach (CMA) for nonlinear bending and post-buckling problems of shells has been proposed in this paper. The CMA approach contains two key stages. *In the first stage*, a coarse mesh-based post-buckling isogeometric analysis is conducted. Accordingly, an initial equilibrium path including a series of initial displacements and a series of initial loads

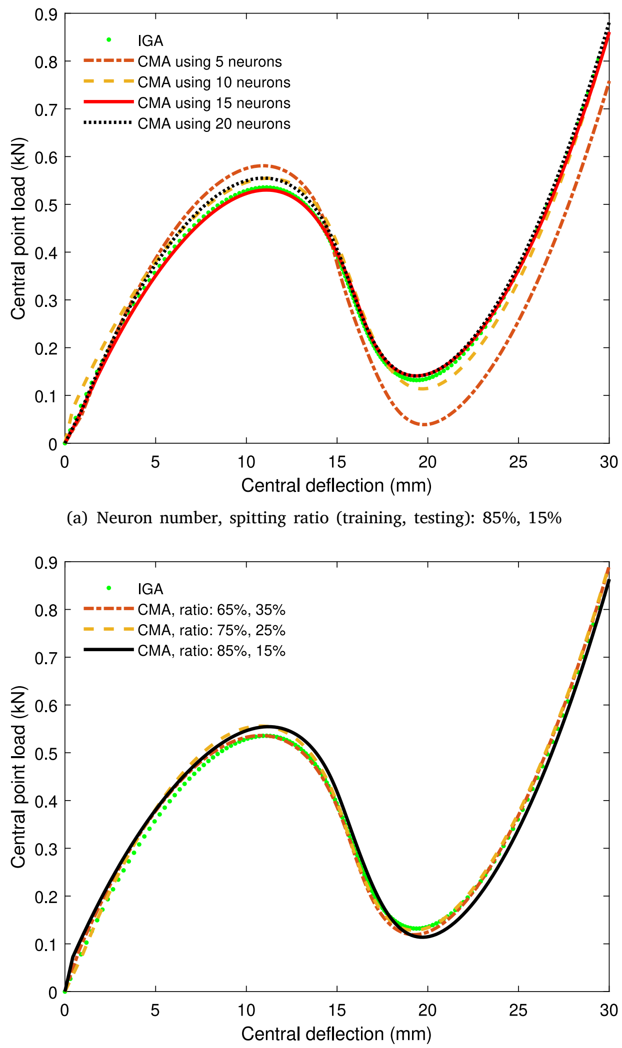

(a) Neuron number, spitting ratio (training, testing): 85%, 15%

(b) Splitting ratio, 10 neurons

Fig. 12. Effect of the network's structure on the CMA solution, delay: 2.

is quickly obtained but incorrect. *In the second stage*, two initial series are considered as the inputs of the trained networks for predictions of displacements and loads. The network outputs are a series of accurate displacements and a series of accurate loads. Therefore, an accurate equilibrium path is achieved upon these two accurate series. Some major conclusions are drawn from the numerical verification as follows:

- High exactness and effectiveness of the CMA approach for post-buckling analysis of shells having snap-through, softening–hardening, and snap-back instabilities and for nonlinear bending analysis of plates were demonstrated. The proposed approach can save 88.4% computational cost compared to the conventional one.
- The present networks were trained utilizing the data generated from post-buckling analyses of curved shells under radial point load with specific materials, geometries, and boundaries. Interestingly, these networks can accurately predict nonlinear responses of not only similar structures and problems but also of other types of structures and problems (such as shells under axial compression or flat plates under bending) with materials, geometries, and boundaries completely different from that used in the data generation. High generalization and exactness of the proposed data-driven models were confirmed. The power and wide application of the CMA approach for nonlinear bending and post-buckling problems of plates and shells were demonstrated.
- Nonlinear auto-regressive exogenous Bayesian neural networks (NARX-BNNs) are recommended for the CMA approach with the following structure. It is recommended to use the CMA approach with at least 10 neurons on the hidden layer and the

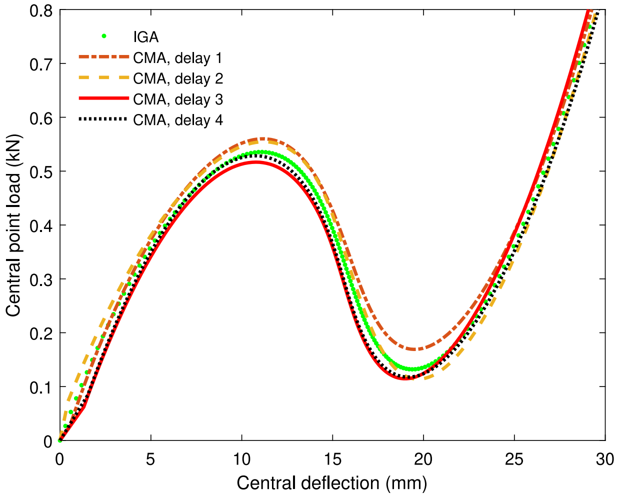

Fig. 13. Effect of the delay number on the CMA solution.

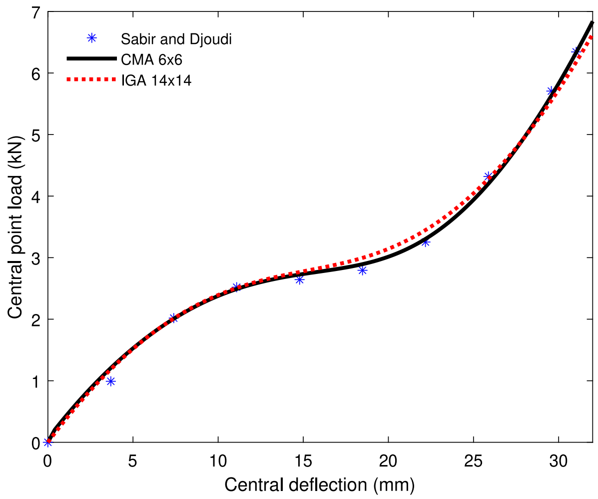

Fig. 14. Analysis of a hinged–hinged panel under central point load, $h = 25.4$ mm.

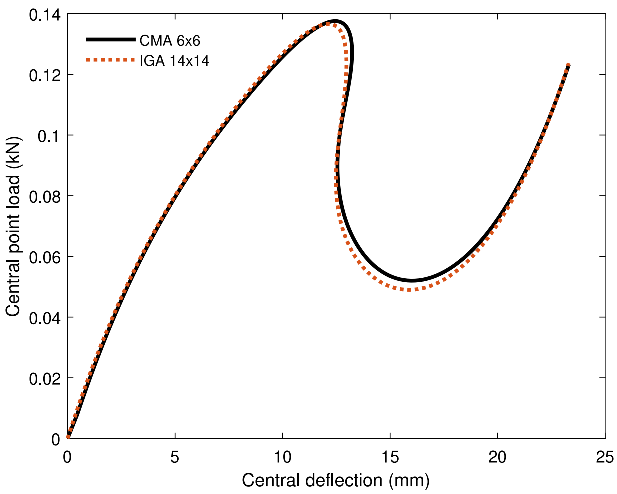

Fig. 15. Analysis of a clamped–hinged panel under central point load, $h = 6.35$ mm.

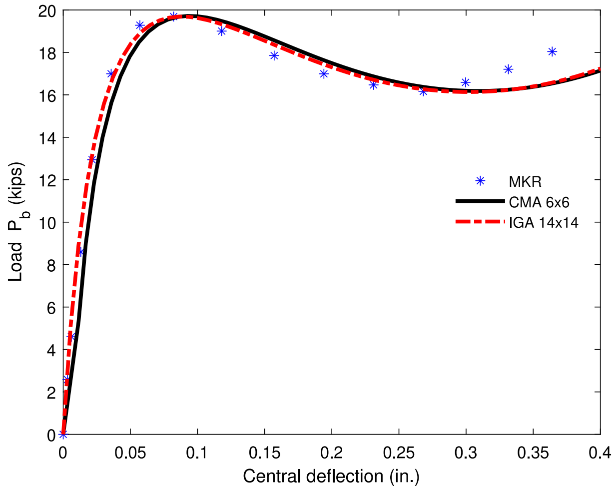

Fig. 16. Analysis of a CCSS panel under axial compression.

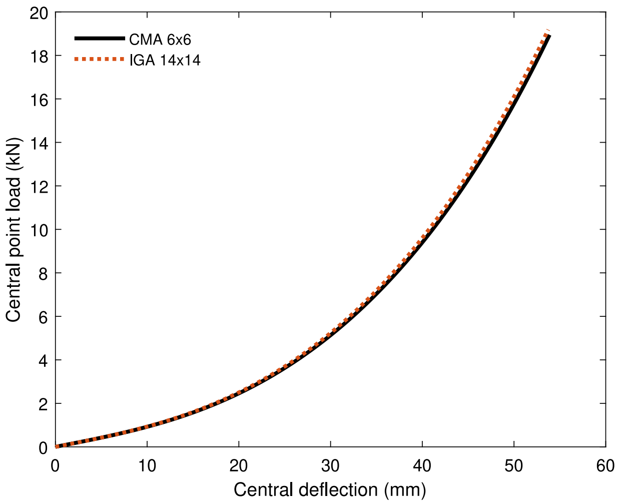

Fig. 17. Analysis of a fully clamped square plate under central point load, $L/h = 30$.

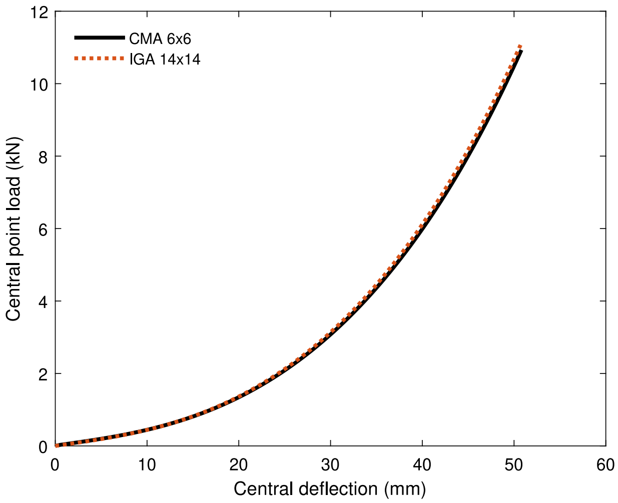

Fig. 18. Analysis of a fully clamped square plate under central point load, $L/h = 40$.

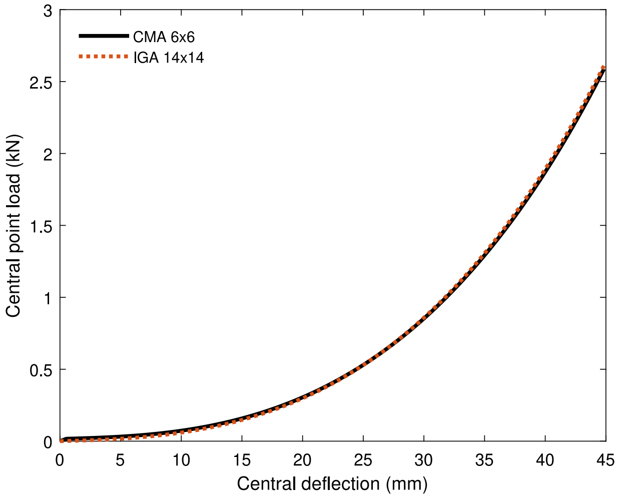

Fig. 19. Analysis of a fully clamped square plate under central point load, $L/h = 100$.

number of delays d is at least equal to 2 to obtain accurate solutions. With these network parameters, the total time for training and applying a network is very low, about 5 s which can be neglected in computing the effectiveness of the approach.
- From the obtained results, it is recommended to use the coarse mesh for flat plates and shallow shells with 6x6 cubic NURBS elements. The finer mesh (or the higher polynomial degree) used in the first stage of the CMA approach may lead to better predictions in the second stage but higher time-consuming.

Upon the notable advantages of the CMA approach, its concept can be applied and extended to a great number of problems in computational mechanics which uses element meshes in the numerical procedure to save time and labor. In fact, the overall efficiency of nonlinear analysis depends not only on mesh refinement (i.e., using a coarse mesh) but also on the adopted nonlinear solver, the step size control, and iteration count. Future works should consider comprehensively and thoroughly these aspects to improve the efficiency of nonlinear analysis. The CMA approach may not be applied to some special cases, in which coarse mesh analysis (or fine mesh analysis) has multiple buckling modes occurring simultaneously or sequentially, for example: ultra-thin shells or plates under compression, modal interaction in post-buckling of structures, and so on.

CRediT authorship contribution statement

Tan N. Nguyen: Writing – review & editing, Methodology, Conceptualization. **Tan Khoa Nguyen:** Validation. **Suppakit Eiadtrong:** Visualization. **Nuttawit Wattanasakulpong:** Data curation. **Mohamed-Ouejdi Belarbi:** Writing – original draft, Supervision, Investigation. **Nader M. Okasha:** Visualization. **Masoomeh Mirrashid:** Investigation. **Aman Garg:** Writing – original draft, Supervision, Investigation.

Declaration of competing interest

The authors declare that they have no known competing financial interests or personal relationships that could have appeared to influence the work reported in this paper.

Data availability

Data will be made available on request.

References

[1] Zhang L.W., Lei Z.X., Liew K.M., Yu J.L., Large deflection geometrically nonlinear analysis of carbon nanotube-reinforced functionally graded cylindrical panels, Comput. Methods Appl. Mech. Engrg. 273 (2014) 1–18.
[2] Nguyen T.N., Lee S., Nguyen P.C., Nguyen-Xuan H., Lee J., Geometrically nonlinear postbuckling behavior of imperfect FG-CNTRC shells under axial compression using isogeometric analysis, Eur. J. Mech. A Solids 84 (2020) 104066.
[3] M. Crisfield, A fast incremental/iterative solution procedure that handles "snap-through", Comput. Struct. 13 (1) (1981) 55–62.
[4] M. Rezaiee-Pajand, R. Naserian, Using residual areas for geometrically nonlinear structural analysis, Ocean Eng. 105 (2015) 327–335.
[5] M. Rezaiee-Pajand, R. Naserian, Geometrical nonlinear analysis based on optimization technique, Appl. Math. Model. 53 (2018) 32–48.
[6] S.G.P. Castro, E.L. Jansen, Displacement-based formulation of Koiter's method, Application to multi-modal post-buckling finite element analysis of plates, Thin-Walled Struct. 159 (2021) 107217.

[7] Y. Sun, K. Tian, R. Li, B. Wang, Accelerated Koiter method for post-buckling analysis of thin-walled shells under axial compression, Thin-Walled Struct. 155 (2020) 106962.

[8] K. Liang, M. Ruess, M. Abdalla, The Koiter–Newton approach using von Kármán kinematics for buckling analyses of imperfection sensitive structures, Comput. Methods Appl. Mech. Engrg. 279 (2014) 440–468.

[9] D. Magisano, K. Liang, G. Garcea, L. Leonetti, M. Ruess, An efficient mixed variational reduced-order model formulation for nonlinear analyses of elastic shells, Internat. J. Numer. Methods Engrg. 113 (4) (2018) 634–655.

[10] Y. Mei, D.E. Hurtado, S. Pant, A. Aggarwal, On improving the numerical convergence of highly nonlinear elasticity problems, Comput. Methods Appl. Mech. Engrg. 337 (2018) 110–127.

[11] R.M.J. Groh, D. Avitabile, A. Pirrera, Generalised path-following for well-behaved nonlinear structures, Comput. Methods Appl. Mech. Engrg. 331 (2018) 394–426.

[12] D. Magisano, L. Leonetti, G. Garcea, How to improve efficiency and robustness of the Newton method in geometrically non-linear structural problem discretized via displacement-based finite elements, Comput. Methods Appl. Mech. Engrg. 313 (2017) 986–1005.

[13] M. Rezaiee-Pajand, H. Estiri, Geometrically nonlinear analysis of shells by various dynamic relaxation methods, World J. Eng. 14 (5) (2017) 381–405.

[14] M. Rezaiee-Pajand, H. Estiri, Finding equilibrium paths by minimizing external work in dynamic relaxation method, Appl. Math. Model. 40 (23) (2016) 10300–10322.

[15] M. Rezaiee-Pajand, H. Afsharimoghadam, An incremental iterative solution procedure without predictor step, Eur. J. Comput. Mech. 27 (1) (2018) 58–87.

[16] A. Maghami, F. Shahabian, S.M. Hosseini, Path following techniques for geometrically nonlinear structures based on Multi-point methods, Comput. Struct. 208 (2018) 130–142.

[17] J.W. Suk, J.H. Kim, Y.H. Kim, A predictor algorithm for fast geometrically-nonlinear dynamic analysis, Comput. Methods Appl. Mech. Engrg. 192 (22) (2003) 2521–2538.

[18] J.H. Kim, Y.H. Kim, A predictor–corrector method for structural nonlinear analysis, Comput. Methods Appl. Mech. Engrg. 191 (8) (2001) 959–974.

[19] A. Maghami, S.M. Hosseini, Intelligent step-length adjustment for adaptive path-following in nonlinear structural mechanics based on group method of data handling neural network, Mech. Adv. Mater. Struct. 29 (20) (2022) 2895–2912, Publisher, Taylor & Francis.

[20] T.N. Nguyen, S. Lee, H. Nguyen-Xuan, J. Lee, A novel analysis-prediction approach for geometrically nonlinear problems using group method of data handling, Comput. Methods Appl. Mech. Engrg. 354 (2019) 506–526.

[21] T.N. Nguyen, H. Nguyen-Xuan, J. Lee, A novel data-driven nonlinear solver for solid mechanics using time series forecasting, Finite Elem. Anal. Des. 171 (2020) 103377.

[22] M. Stoffel, F. Bamer, B. Markert, Artificial neural networks and intelligent finite elements in non-linear structural mechanics, Thin-Walled Struct. 131 (2018) 102–106.

[23] V. Papadopoulos, G. Soimiris, D. Giovanis, M. Papadrakakis, A neural network-based surrogate model for carbon nanotubes with geometric nonlinearities, Comput. Methods Appl. Mech. Engrg. 328 (2018) 411–430.

[24] M. Bazmara, M. Silani, M. Mianroodi, M. Sheibanian, Physics-informed neural networks for nonlinear bending of 3D functionally graded beam, Structures 49 (2023) 152–162.

[25] T.N. Nguyen, J. Lee, L. Dinh-Tien, L. Minh Dang, Deep learned one-iteration nonlinear solver for solid mechanics, Internat. J. Numer. Methods Engrg. 123 (8) (2022) 1841–1860, Publisher, John Wiley & Sons, Ltd.

[26] G. Marcjasz, B. Uniejewski, R. Weron, On the importance of the long-term seasonal component in day-ahead electricity price forecasting with NARX neural networks, Int. J. Forecast. 35 (4) (2019) 1520–1532.

[27] Y. Raptodimos, I. Lazakis, Application of NARX neural network for predicting marine engine performance parameters, Ships Offshore Struct. 15 (4) (2020) 443–452, Publisher, Taylor & Francis.

[28] M. Wei, M. Ye, J.B. Li, Q. Wang, X. Xu, State of Charge Estimation of Lithium-Ion Batteries Using LSTM and NARX Neural Networks, IEEE Access 8 (2020) 189236–189245.

[29] F. Di Nunno, F. Granata, Groundwater level prediction in Apulia region (Southern Italy) using NARX neural network, Environ. Res. 190 (2020) 110062.

[30] A. Cheng, Y.M. Low, Improved generalization of NARX neural networks for enhanced metamodeling of nonlinear dynamic systems under stochastic excitations, Mech. Syst. Signal Process. 200 (2023) 110543.

[31] Y.W. Lee, T.L. Chang, Application of NARX neural networks in thermal dynamics identification of a pulsating heat pipe, Energy Convers. Manage. 50 (4) (2009) 1069–1078.

[32] C.A. Perez-Ramirez, J.P. Amezquita-Sanchez, M. Valtierra-Rodriguez, H. Adeli, A. Dominguez-Gonzalez, R.J. Romero-Troncoso, Recurrent neural network model with Bayesian training and mutual information for response prediction of large buildings, Eng. Struct. 178 (2019) 603–615.

[33] T.N. Nguyen, C.H. Thai, A.T. Luu, H. Nguyen-Xuan, J. Lee, NURBS-based postbuckling analysis of functionally graded carbon nanotube-reinforced composite shells, Comput. Methods Appl. Mech. Engrg. 347 (2019) 983–1003.

[34] N. Nguyen-Thanh, K. Zhou, X. Zhuang, P. Areias, H. Nguyen-Xuan, Y. Bazilevs, T. Rabczuk, Isogeometric analysis of large-deformation thin shells using RHT-splines for multiple-patch coupling, Spec. Issue Isogeometric Anal., Prog. Challenges 316 (2017) 1157–1178.

[35] L. Leonetti, F. Liguori, D. Magisano, G. Garcea, An efficient isogeometric solid-shell formulation for geometrically nonlinear analysis of elastic shells, Comput. Methods Appl. Mech. Engrg. 331 (2018) 159–183.

[36] J.C. Simo, D.D. Fox, M.S. Rifai, On a stress resultant geometrically exact shell model. Part III, Computational aspects of the nonlinear theory, Comput. Methods Appl. Mech. Engrg. 79 (1) (1990) 21–70.

[37] V.L. Tran, D.K. Thai, S.E. Kim, Application of ANN in predicting ACC of SCFST column, Compos. Struct. 228 (2019) 111332.

[38] S. Mouloodi, H. Rahmanpanah, S. Gohari, C. Burvill, H.M. Davies, Feedforward backpropagation artificial neural networks for predicting mechanical responses in complex nonlinear structures, A study on a long bone, J. Mech. Behav. Biomed. Mater. 128 (2022) 105079.

[39] I. M Nikbin, R.S. Rahimi, H. Allahyari, A new empirical formula for prediction of fracture energy of concrete based on the artificial neural network, Eng. Fract. Mech. 186 (2017) 466–482.

[40] F. Dan Foresee, M. Hagan, Gauss-newton approximation to bayesian learning, in: Proceedings of International Conference on Neural Networks (ICNN'97), vol. 3, 1997, pp. 1930–1935, vol.3.

[41] A.B. Sabir, M.S. Djoudi, Shallow shell finite element for the large deflection geometrically nonlinear analysis of shells and plates, Thin-Walled Struct. 21 (3) (1995) 253–267.

[42] T.M. Le, H. Nguyen-Xuan, L. Leonetti, A new paradigm coupling element-wise discrete-strain gaps with patch-wise reduced integration for efficient isogeometric nonlinear Kirchhoff–Love shell analysis, Comput. Methods Appl. Mech. Engrg. 436 (2025) 117667.

[43] K.M. Liew, Z.X. Lei, J.L. Yu, L.W. Zhang, Postbuckling of carbon nanotube-reinforced functionally graded cylindrical panels under axial compression using a meshless approach, Comput. Methods Appl. Mech. Engrg. 268 (2014) 1–17.